Video Article

Demonstration of a Hyperlens-integrated Microscope and Super-resolution Imaging

Dasol Lee*[1], Minkyung Kim*[1], Sunae So*[1], Inki Kim[1], Gwanho Yoon[1], Kyunghoon Kim[2], Junsuk Rho[1,3]

[1]Department of Mechanical Engineering, Pohang University of Science and Technology (POSTECH)

[2]School of Mechanical Engineering, Sungkyunkwan University

[3]Department of Chemical Engineering, Pohang University of Science and Technology (POSTECH)

*These authors contributed equally

Correspondence to: Kyunghoon Kim at kenkim@skku.edu, Junsuk Rho at jsrho@postech.ac.kr

URL: https://www.jove.com/video/55968
DOI: doi:10.3791/55968

Keywords: Engineering, Issue 127, Super-resolution far-field imaging, diffraction limit, hyperbolic metamaterials, hyperlens, real-time imaging, novel microscope, nanofabrication

Date Published: 9/8/2017

Citation: Lee, D., Kim, M., So, S., Kim, I., Yoon, G., Kim, K., Rho, J. Demonstration of a Hyperlens-integrated Microscope and Super-resolution Imaging. *J. Vis. Exp.* (127), e55968, doi:10.3791/55968 (2017).

Abstract

The use of super-resolution imaging to overcome the diffraction limit of conventional microscopy has attracted the interest of researchers in biology and nanotechnology. Although near-field scanning microscopy and superlenses have improved the resolution in the near-field region, far-field imaging in real-time remains a significant challenge. Recently, the hyperlens, which magnifies and converts evanescent waves into propagating waves, has emerged as a novel approach to far-field imaging. Here, we report the fabrication of a spherical hyperlens composed of alternating silver (Ag) and titanium oxide (TiO_2) thin layers. Unlike a conventional cylindrical hyperlens, the spherical hyperlens allows for two-dimensional magnification. Thus, incorporation into conventional microscopy is straightforward. A new optical system integrated with the hyperlens is proposed, allowing for a sub-wavelength image to be obtained in the far-field region in real time. In this study, the fabrication and imaging setup methods are explained in detail. This work also describes the accessibility and possibility of the hyperlens, as well as practical applications of real-time imaging in living cells, which can lead to a revolution in biology and nanotechnology.

Video Link

The video component of this article can be found at https://www.jove.com/video/55968/

Introduction

A desire to observe biomolecules in living cells led to the invention of microscopy, and the advent of microscopy propagated the revolution of various fields, such as biology, pathology, and material science, over last few centuries. However, further advancement of research has been restricted by diffraction, which limits the resolution of conventional microscopes to about half of the wavelength[1]. Therefore, super-resolution imaging to overcome the diffraction limit has been an interesting research area in recent decades.

As the diffraction limit is attributed to the loss of the evanescent waves that contain sub-wavelength information on objects, early studies have been conducted to keep evanescent waves from fading away or to recover them[2,3]. The effort to overcome the diffraction limit was first reported with near-field scanning optical microscopy, which collects the evanescent field in close proximity to the object before it is dissipated[2]. However, as scanning the whole image region and reconstructing it takes a long time, it cannot be applied to real-time imaging. Although another approach based on the "superlens," which amplifies evanescent waves, provides the possibility of real-time imaging, sub-wavelength imaging is only capable in the near-field region and cannot reach far beyond the objects[4,5,6,7].

Recently, the hyperlens has emerged as a novel approach to real-time far-field optical imaging[8,9,10,11,12]. The hyperlens, which is made of highly anisotropic hyperbolic metamaterials[13], exhibits a flat hyperbolic dispersion so that it supports high spatial information with the same phase velocity. Furthermore, due to the momentum conservation law, the high transverse wavevector is gradually compressed as the wave goes through the cylindrical geometry. This magnified information thus can be detected by a conventional microscope in the far-field region. This is of particular importance to real-time far-field imaging, as it does not require any point-by-point scanning or image reconstruction. Moreover, the hyperlens can be used for applications other than imaging, including nanolithography. Light that passes through the hyperlens in the reverse direction will be focused onto a sub-diffraction area due to the time-reversal symmetry[14,15,16].

Here, we report on a spherical hyperlens that magnifies two-dimensional information at the visible frequency. Unlike conventional cylindrical geometry, the spherical hyperlens magnifies objects in two lateral dimensions, facilitating practical imaging applications. The fabrication method and imaging setup with the hyperlens are presented in detail for the reproduction of a high-quality hyperlens. A sub-wavelength object is inscribed on the hyperlens for the sake of proving its super-resolving power. It is confirmed that small features of inscribed objects are magnified by the hyperlens. Thus, clearly resolved images are obtained in the far-field region in real time. This new type of spherical hyperlens, with its

ease of integration with conventional microscopy, provides the possibility of practical imaging applications, leading to the dawn of a new era in biology, pathology, and general nanoscience.

Protocol

1. Substrate Preparation

1. Obtain highly refined quartz wafer. For the fabrication reported here, use a wafer with a 500 µm thickness.
2. Spin-coat the quartz wafer with a positive photoresist at 2,000 rpm and bake for 60 s at 90 °C.
   NOTE: The positive photoresist layer is coated to prevent damage during the subsequent cutting step.
3. Use a dicing machine to cut the wafer with photoresist into small pieces 20 x 20 mm^2 in size.
4. Blow using a compressed nitrogen gun to remove particulates resulting from the cutting step.
5. Place it in an ultrasonic bath in de-ionized (DI) water for 5 min at 45 °C. Remove the photoresist layer using an ultrasonic bath in acetone for 5 min at 45 °C. Clean the substrate using two ultrasonic baths, acetone and isopropyl alcohol, each for 5 min at 45 °C.
6. Dry the substrate with a compressed nitrogen gun.

2. Etching the Mask Pattern

1. Load the clean quartz substrates into a high-vacuum electron beam evaporation system. Ensure that substrate rotation is enabled.
2. Deposit the chromium layer with a deposition rate of 2 Å/s.
   NOTE: A layer at least 100 nm-thick should be deposited for the etching mask to prevent pinholes made from deposition.
3. Press the vent button to vent the chamber and mount a sample on the focused ion beam (FIB) holder using conducting copper tape.
4. Load the FIB holder into the FIB chamber.
5. Close the chamber door and press the pump button to evacuate the chamber.
6. Select "beam on" under the beam control tab and set the ion beam current (7.7 pA) and acceleration voltage (30 kV) for FIB mode.
7. Turn on the ion beam system.
8. Select "beam on" under the beam control tab to turn on the electron beam and focus the image with low magnification using software.
9. Set the working distance (WD) at 4 mm under the navigation tab in scanning electron microscope (SEM) mode.
10. Set the tilt angle of the holder to 52° and take the SEM images at different magnifications before hole array mask pattern fabrication.
11. Under the patterning tab, choose the patterning region and make a 50 nm hole array on the chromium layer.
    NOTE: There are simple patterning tools accessible under the patterning tab. More complex geometry and exposure control can be achieved by importing bitmaps or generating scripts.
12. After finishing, turn off the electron beam and ion beam systems and cool down the system.
13. Press the vent button and vent the chamber with nitrogen gas. Take the holder out of the chamber.
14. Close the chamber door and evacuate the chamber by pressing the pump button.

3. Wet-etching Process and Removal of the Mask Layer

1. Put the patterned substrate into 1:10 buffered oxide etchant for 5 min.
   NOTE: The quartz is selectively and isotropically wet-etched by the etchant and forms a spherical shape. The shape of the lens can be obtained with the etching mask, and the diameter is precisely controlled by the etching time. A better spherical shape can be formed with a smaller pattern diameter. A 1.5 µm-diameter hemisphere can be obtained within 5 min.
2. Put the patterned substrate into DI water to clean the buffered oxide etchant (5 min, two times).
   NOTE: Buffered oxide etchant can be dangerous, so be careful when using this etchant.
3. Dry the sample with compressed nitrogen gas.
4. Put the patterned substrate into CR-7 chromium etchant to remove the chromium mask layer.
   NOTE: After removing the chromium layer, a spherical patterned substrate 1.5 µm in diameter can be obtained.
5. Put the patterned substrate into DI water to clean it (5 min).

4. Multilayer Deposition and Nano-sized Object Inscription

NOTE: A pair of layers are deposited on the spherical quartz substrate. Here, Ag and TiO_2 are used as the deposition materials. Ag and TiO_2 are deposited alternately at a thickness of 15 nm.

1. Press the vent button of the electron beam evaporation system and wait until the vent is over.
2. Load the patterned substrate into a high-vacuum electron beam evaporation system after the vent.
3. Close the chamber door and evacuate the chamber to a vacuum degree of 10^{-7} Torr by pressing the pump button.
   NOTE: The vacuum condition should be kept at 10^{-7} Torr to reduce the scattering from the surface roughness.
4. Deposit the Ag layer with a growth rate of 1 Å/s and deposit a 15 nm-thick Ag layer.
5. After the deposition of the Ag layer, cool down the substrate for 5 min.
6. Change the pocket of the electron beam evaporation system by choosing another crucible and deposit the TiO_2 layer with a growth rate of 1 Å/s. Deposit a 15 nm-thick TiO_2 layer.
   NOTE: During the deposition process, the film growth rate is kept low to maintain the surface roughness uniformity.
7. After the deposition of the TiO_2 layer, cool down the substrate for 5 min.
8. Repeat steps 4.4 - 4.7 for tens of cycles to deposit a multilayer of Ag and TiO_2.

NOTE: At this point, the hyperlens fabrication is over. The next step is for making an arbitrary sub-diffraction-limited feature for testing the hyperlens imaging ability. Nanometer-sized apertures and slits are inscribed by FIB milling.

9. Change the pocket of the electron beam evaporation system and deposit the chromium layer at a thickness of 50 nm.
10. After the deposition of a Cr layer, turn off the electron beam evaporation system. Press the vent button and vent the chamber by introducing nitrogen gas.
11. After the vent, open the chamber door and take the mount holder out of the chamber. Strip off the fabricated hyperlens device.
12. Close the chamber door and evacuate the chamber by pressing the pump button.
13. Mount the hyperlens deposited with chromium into the FIB milling system and pattern a nano-sized structure, per the manufacturer's instructions.

5. Setting Up the Imaging System and Imaging Procedure

1. Place a conventional transmission-type optical microscope on the optical table.
   NOTE: Here, an inverted optical microscope was used as the main body.
2. Connect a white-light source to the microscope illumination path using an adapter.
3. Place an optical bandpass filter centered at 410 nm.
   NOTE: The bandpass filter selectively penetrates the specific wavelength of light; here, 410 nm light is illuminated on the sample. A hyperlens consisting of Ag and TiO_2 has high performance at a 410 nm wavelength. The simulation result (**Figure 2c**) shows the performance of the hyperlens, which satisfies the hyperbolic dispersion relation at 410 nm light.
4. Select a high-magnification oil-immersion objective lens. Use a high-quality CCD camera to obtain the images.
   NOTE: This optical setting just puts the bandpass filter into the light illumination path to sort out the 410 nm wavelength light. A specific wavelength of light can be illuminated on the sample without using white light, but in a normal laboratory, optical microscopes may have a white-light source for the observation of samples through bright-field or fluorescence imaging.
5. Place a drop of immersion oil on the objective lens. Place a hyperlens on the sample stage and capture images.
   NOTE: The inscribed nano-sized objects on the inner surface of the hyperlens can be illuminated with 410 nm light. With the hyperlens, the nano-sized objects will be magnified and be captured by the objective lens and imaged by CCD camera.

Representative Results

The ability of the hyperlens device to resolve sub-diffraction features relies on its uniformity and on a high-quality fabrication. Here, a hyperlens is composed of a multilayer of Ag and TiO_2 deposited alternately. **Figure 2a** shows the SEM image of a well-made hyperlens[17]. The cross-sectional image shows that the multilayer of Ag and Ti_3O_5 thin film is deposited with uniform thickness on the hemispherical quartz substrate. The surface roughness of the final hyperlens structure is less than 1.5 nm root mean square (r.m.s).

We used TiO_2 instead of Ti_3O_5 as a dielectric since both materials, which have high refractive indices over 2, give rise to effective hyperbolic dispersion when stacked with silver. As mentioned in the **Protocol**, a hyperlens consisting of Ag and TiO_2 has a great performance at 410 nm because the dispersion relation of the stacked multilayer of Ag and TiO_2 has a hyperbolic dispersion curve, as shown **Figure 2b**. In principle, waves with high spatial wavevector components can propagate in such a hyperbolic medium along the radial direction of the hyperlens. In other words, the small features having high-frequency components, which cannot be captured by conventional optics, can propagate to the far-field through the hyperlens. **Figure 2c** shows the simulated field distribution in the hyperlens using a finite element (FEM) simulation tool. The design, material properties, and inscribed nanostructures of the simulation model are set identically with those of the fabricated hyperlens. Two holes 50 nm in diameter are inscribed on the chromium layer, with a distance of 150 nm. The top of the hyperlens is illuminated by 410 nm light, and the light from the hyperlens contains the magnified image of the object, where the magnification is determined by the ratio between the inner radius and the outer radius of the hyperlens. The magnified image of the sub-diffraction-limited object can be captured by a conventional objective lens and imaged.

The measurement of the diffraction-unlimited image using a hyperlens is performed through a simple optical system. **Figure 3a** shows the schematic of the hyperlens imaging system. Conventional microscopy can be used as a mainframe, with slight differences. The illumination path is the transmission type and the white-light source is placed with a proper bandpass filter. The illumination light is collected by a condenser or focusing lens and delivered to the object plane. The sample is placed on the inner surface of the hyperlens in a hyperlens imaging system, while the sample is placed on the slide glass in conventional optical microscopy. The objects in the hyperlens are illuminated, and the image then propagates through the hyperlens. Finally, the image is captured by an objective lens and CCD camera. The hyperlens-implemented optical system is shown in **Figure 3b**. With simple additional components, such as a source and filter, the hyperlens can easily be implemented in a conventional microscope system.

The real images captured through a hyperlens are shown in **Figure 4**. **Figure 4a** and **4d** depict two sets of the SEM images of sub-wavelength structures, consisting of a hole and line inscribed in the chromium layer of the hyperlens. The gap sizes are from 160 - 180 nm in each case. In conventional microscopy, these sub-diffraction structures cannot be resolved because of to the diffraction limit. On the other hand, the small features are clearly resolved with the hyperlens. **Figure 4b and 4e** show the obtained optical images using the hyperlens-based system, and the cross-sectioned intensity profiles (red dashed line) are shown in **Figure 4c and 4f**, respectively. Cross-sectional intensity graphs show separations of 363 and 346 nm (**Figure 4c**) and 333 nm (**Figure 4f**), respectively, corresponding to a magnification of 2.1, determined by the ratio between the inner and outer radius of the hyperlens.

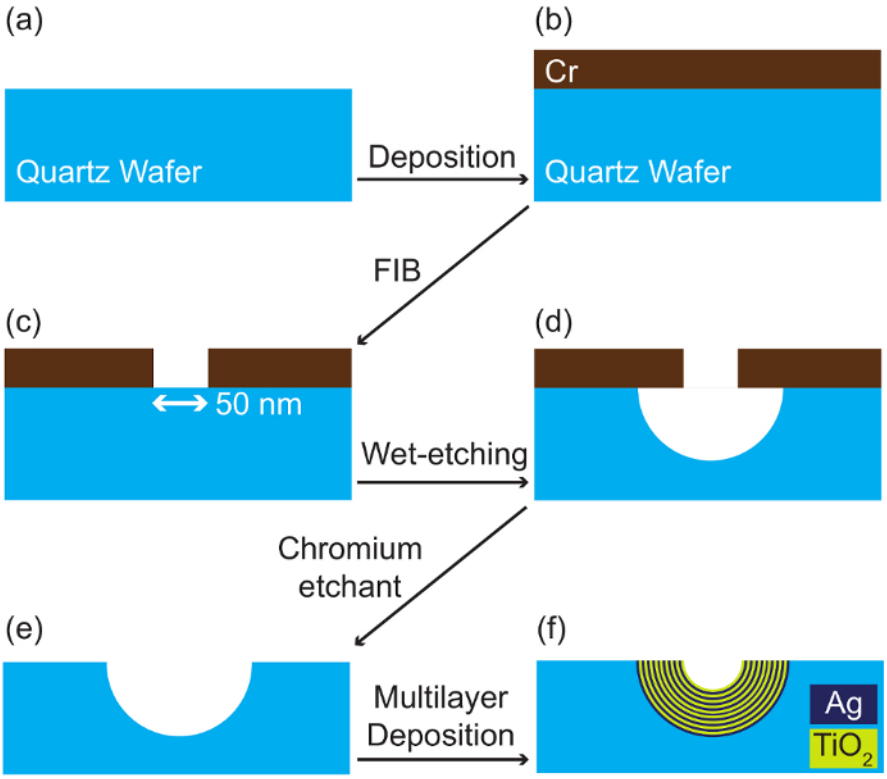

Figure 1: Schematic of the Hyperlens Fabrication Process. (**a**) The fabrication begins with the preparation of refined quartz wafer. (**b**) On the quartz wafer, a chromium layer 100 nm thick is deposited by an electron beam evaporation system. (**c**) To make a mask pattern for a wet-etching process, a 50 nm-diameter hole is patterned on the chromium layer using an FIB milling system. (**d**) An isotropic wet-etching process is carried out using the chromium layer. A hemispherical shape is formed on the quartz wafer. (**e**) The removal of the chromium layer is done with a chromium etchant. (**f**) On the hemispherical surface is a multilayer of Ag and TiO_2 deposited alternately, with a thickness of 15 nm. Please click here to view a larger version of this figure.

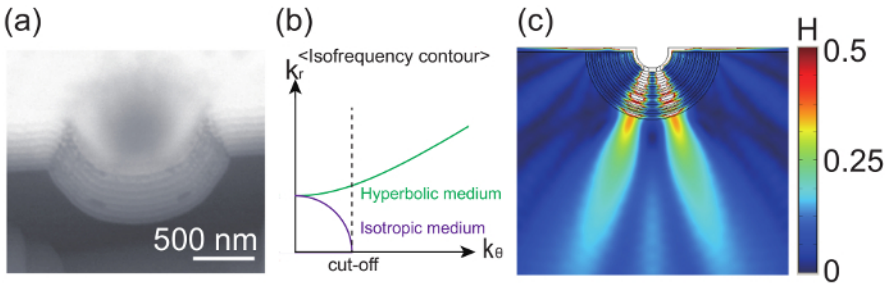

Figure 2: Fabrication and Simulation Results of the Hyperlens. (**a**) Cross-sectioned SEM image of the fabricated hyperlens. Each layer of Ag and TiO_2 with a 15 nm thickness is well-deposited, with uniformity, and the roughness of final hyperlens is less than 1.5 r.m.s. This figure has been modified from reference[17]. (**b**) Isofrequency contour of the hyperlens (green line) and isotropic medium (purple line). The hyperlens has a hyperbolic shape of dispersion relation that can propagate the high-frequency component (small features, higher than cut-off value) to the far field. However, isotropic medium-like conventional optics has a circular dispersion relation and cannot propagate over the cut-off frequency. (**c**) Simulation result of the hyperlens. The result shows the magnetic field distribution from small features inside the hyperlens inner surface. The sub-diffractional object is magnified and propagated to the far field through the hyperlens. Please click here to view a larger version of this figure.

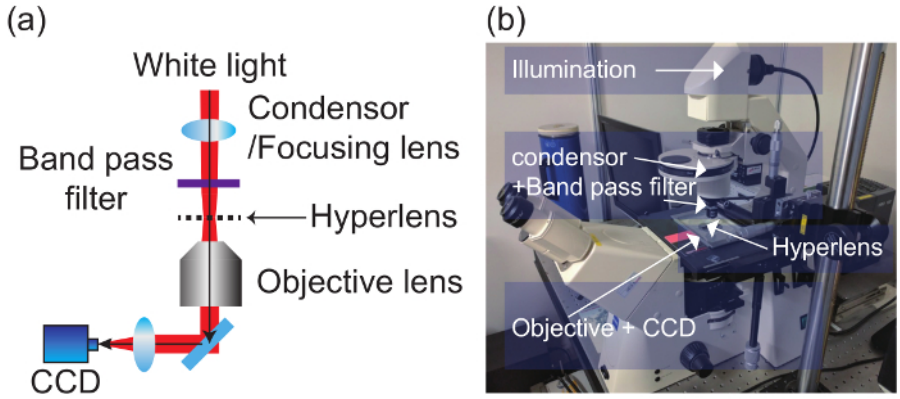

Figure 3: Hyperlens-implemented Imaging System Schematic. (**a**) A broadband white-light source is used to illuminate the sample. The light passes through the bandpass filter and a specific wavelength of light is selected. Here, 410 nm light is used as the illumination light. The hyperlens is implemented easily on the object plane and through the objective lens and CCD camera so that the small object on the hyperlens is captured. (**b**) Hyperlens-implemented imaging system. A conventional inverted microscope body is used as a mainframe, and the hyperlens is added for super-resolution imaging. Please click here to view a larger version of this figure.

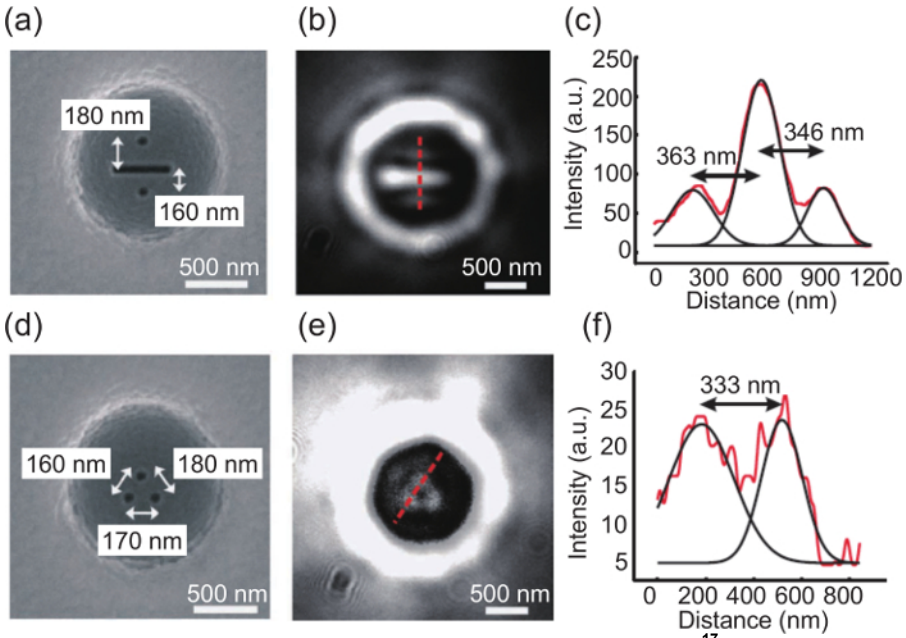

Figure 4: Fabrication Result and Simulation Results of the Hyperlens[17]. (**a**) SEM image of an object with two dots separated by a line structure. Each dot has distances of 180 nm and 160 nm. (**b**) Optical image captured through the hyperlens. The small object in the hyperlens is magnified and captured. The sub-diffraction limited features are resolved. (**c**) Along the red dashed line, the cross-sectioned intensity profile is measured. The cross-sectional intensity profiles show separations of 363 and 346 nm. (d) SEM image of another object, with three dots 160, 170, and 180 nm from each other. (**e**) Optical image captured through the hyperlens. (**f**) Cross-sectioned intensity profile of the red dashed line in (**e**). The cross-sectional intensity profile shows a separation of 333 nm. Cross-sectional intensity profiles correspond to the 2.1X magnification factor of the hyperlens. This figure has been modified from refefence[17]. Please click here to view a larger version of this figure.

Discussion

The fabrication of a hyperlens includes three major steps: defining hemispherical geometry into the quartz substrate through a wet-etching process, stacking the metal and dielectric multilayer using an electron beam evaporation system, and inscribing the object on the Cr layer. The most important step is the second, since it can significantly affect quality of the hyperlens. In the thin-film deposition process, there are two conditions that require special care for a clear super-resolved image. Stacking the multilayer conformally is one of the crucial issues, as the non-conformal deposition of the multilayer leads to a deviation from the perfect spherical shape. If the film deposition is not slow enough, the film thickness at the center and that at the edge of the hemispheric geometry tend to differ due to the angled nature of electron beam evaporation. The spatially different film thickness gives rise to spatially dependent magnification and causes image distortion. Therefore, the film deposition rate should be as slow as possible (less than 0.1 nm/s) to achieve a conformal multilayer.

Another possible factor that can bring out an imperfect image is the surface roughness, since a rough surface increases the probability of light scattering. It has been reported that the inclusion of a thin layer of a high-surface energy material has a wetting effect, drastically reducing the percolation of silver[18]. Here, the TiO_2 layer works as the wetting material. Silver deposited on the TiO_2 layer tends to be flatter than usual. In addition, the vacuum condition should be less than 10^{-7} Torr throughout the deposition process for an even and smooth multilayer. Agglomeration

of silver during the electron beam evaporating can also make the surface rough. Since the agglomeration is suppressed at low temperatures, the film deposition can be performed in cryogenic conditions controlled by liquid nitrogen. After the thin-film deposition, we examined the surface roughness of the fabricated structure to ensure the smooth surface using AFM and confirmed that the surface roughness is less than 1.5 nm.

Even if all three conditions are carefully controlled, a perfect image is unobtainable, even under ideal fabrication. First, as with any other conventional optical system, the hyperlens-based optical system, which includes hyperlens and conventional high-NA optics, is subject to conventional aberrations, such as spherical aberrations. Also, although spherical structures of the hyperlens enable two-dimensional super-resolution imaging under unpolarized light, the spherical geometry gives rise to aberrations. For example, when the object is composed of two holes and a slit inscribed on the Cr layer, they are not on the same object plane. Therefore, one of the objects can be in focus while the others are not. This partial focusing also originates from the discordance of the sample and the optical axis of the subsequent high-NA imaging. Apart from this spatial-dependent resolution, additional blurring is observed due to the fringe effect, which stems from the residual coherence in the illumination light.

Furthermore, the breakdown of the effective medium approximation limits the resolution. For waves whose transverse wave vector component is too large compared to the vacuum wavelength, the effective wavelength in the hyperlens becomes smaller, and sometime it becomes comparable to the film thickness. Therefore, effective medium approximation is not valid anymore. As the effective wavelength approaches 2d, where d is the thickness of the layers, the dispersion curve considerably deviates from the hyperbolic shape, and the waves cannot propagate. This limits the resolution within 60 nm for the specific hyperlens-based system shown here. We also should mention that, although the hyperlens delivers images in the far-field, the object should be placed in a near-field. Otherwise, evanescent waves carrying sub-diffraction features cannot reach the hyperbolic medium.

Despite the fundamental limitations to the resolution of the hyperlens, we succeeded in improving imaging quality by mimicking the smooth and perfect spherical structure of the hyperlens. The smooth interface ensures lower scattering and less image distortion, while the conformal structure reduces the spatial-dependent aberration. Furthermore, since super-resolution imaging using hyperlenses originates from the extraordinary dispersion relation, it is free from the use of fluorescence or other complicated mechanisms, such as the stochastic method. Consequently, a hyperlens does not require post-processing and makes real-time imaging possible. It also does not involve intricate experimental components, working as an optics module that can easily be integrated with a conventional optics setup, as demonstrated. Moreover, thin-film process can be used to stack a wide range of materials, with the thickness controllable on a nanometer-scale. Therefore, a hyperlens working at a different wavelength regime can be fabricated using different materials.

Here, we present the fabrication process of a hyperlens and its optical setup for imaging. We also experimentally report label-free sub-diffraction images in real-time using a hyperlens-based optical system. Since the hyperlens has a simple spherical geometry, there are other degrees of freedom to reduce constraints in the imaging environment. For example, we can improve the practicality by adopting a scalable fabrication method or expand its versatility by adding additional steps to the fabrication to enable *in vitro* imaging applications. The use of hyperlenses will allow scientists to observe biophysical dynamics occurring on the nanoscale in real-time. It can be considered the next generation of the super-resolution imaging platform, for use in various applications such as biology, medical science, and material engineering.

Disclosures

The authors declare that they have no competing financial interests.

Acknowledgements

This work is financially supported by Young Investigator program (NRF-2015R1C1A1A02036464), Engineering Research Center program (NRF-2015R1A5A1037668) and Global Frontier program (CAMM-2014M3A6B3063708), M.K., S.S., I.K. acknowledge the Global Ph.D. Fellowships (NRF-2017H1A2A1043204, NRF-2017H1A2A1043322, NRF-2016H1A2A1906519) through the National Research Foundation of Korea (NRF) grant funded by the Ministry of Science, ICT and Future Planning (MSIP) of Korean government.

References

1. Abbe, E. Beiträge zur Theorie des Mikroskops und der mikroskopischen Wahrnehmung. *Archiv für mikroskopische Anatomie.* **9** (1), 413-418 (1873).
2. Dürig, U., Pohl, D. W., Rohner, F. Near-field optical-scanning microscopy. *J Appl Phys.* **59** (10), 3318-3327 (1986).
3. Pendry, J. B. Negative Refraction Makes a Perfect Lens. *Phys Rev Lett.* **85** (18), 3966-3969 (2000).
4. Fang, N., Liu, Z., Yen, T.-J., Zhang, X. Regenerating evanescent waves from a silver superlens. *Opt Express.* **11** (7), 682-687 (2003).
5. Fang, N., Lee, H., Sun, C., Zhang, X. Sub-Diffraction-Limited Optical Imaging with a Silver Superlens. *Science.* **308** (5721), 534-537 (2005).
6. Melville, D. O. S., Blaikie, R. J. Super-resolution imaging through a planar silver layer. *Opt Express.* **13** (6), 2127-2134 (2005).
7. Taubner, T., Korobkin, D., Urzhumov, Y., Shvets, G., Hillenbrand, R. Near-Field Microscopy Through a SiC Superlens. *Science.* **313** (5793), 1595-1595 (2006).
8. Jacob, Z., Alekseyev, L. V., Narimanov, E. Optical Hyperlens: Far-field imaging beyond the diffraction limit. *Opt Express.* **14** (18), 8247-8256 (2006).
9. Lee, H., Liu, Z., Xiong, Y., Sun, C., Zhang, X. Development of optical hyperlens for imaging below the diffraction limit. *Opt Express.* **15** (24), 15886-15891 (2007).
10. Liu, Z., Lee, H., Xiong, Y., Sun, C., Zhang, X. Far-Field Optical Hyperlens Magnifying Sub-Diffraction-Limited Objects. *Science.* **315** (5819), 1686-1686 (2007).
11. Kim, M., Rho, J. Metamaterials and imaging. *Nano Converg.* **2** (1), 22 (2015).
12. Byun, M. *et al.* Demonstration of nanoimprinted hyperlens array for high-throughput sub-diffraction imaging. *Sci Rep.* **7,** 46314 (2017).
13. Shekhar, P., Atkinson, J., Jacob, Z. Hyperbolic metamaterials: fundamentals and applications. *Nano Converg.* **1** (1), 14 (2014).

14. Liu, L. *et al.* Sub-diffraction demagnification imaging lithography by hyperlens with plasmonic reflector layer. *RSC Advances.* **6** (98), 95973-95978 (2016).
15. Sun, J., Xu, T., Litchinitser, N. M. Experimental demonstration of demagnifying hyperlens. *Nano Lett.* **16** (12), 7905-7909 (2016).
16. Kim, M. *et al.* Deep sub-wavelength nanofocusing of UV-visible light by hyperbolic metamaterials. *Sci Rep.* **6**, 38645 (2016).
17. Rho, J. *et al.* Spherical hyperlens for two-dimensional sub-diffractional imaging at visible frequencies. *Nat Commun.* **1**, 143 (2010).
18. Chen, W. *et al.* Ultra-thin ultra-smooth and low-loss silver films on a germanium wetting layer. *Opt Express.* **18** (5), 5124-5134 (2010).

